Intensity dependent properties of photo-induced light scattering in ferroelectric $Sr_{0.61}Ba_{0.39}Nb_2O_6$:Ce

M Goulkov[1], O Fedorenko[1], Th Woike[2], T Granzow[2,4], M Imlau[3] and M Wöhlecke[3]

[1] Institute of Physics, Science Avenue 46, 03650, Kiev-39, Ukraine
[2] Institute of Mineralogy, University of Cologne, Zülpicherstraße 49b, D-50674 Cologne, Germany
[3] Department of Physics, University Osnabrück, Barbarastraße 7, D-49069 Osnabrück, Germany

Abstract

An experimental study of intensity dependent properties of photo-induced scattering (beam fanning) in Ce-doped $Sr_{0.61}Ba_{0.39}Nb_2O_6$, both field-free and under the action of external electric fields, is reported. A new effect, the spontaneous local reorientation of the scattering pattern, is found and is attributed to optically induced local switching of the polar structure. It is demonstrated that features of scattering observed at high intensities are governed by changes of ferroelectric and photorefractive properties of SBN in the beam area during heating up to the vicinity of the phase transition by coherent illumination.

1. Introduction

Optical recording of phase gratings in photoferroelectrics without a centre of inversion is provided via the photorefractive effect [1]. Recording is accompanied by nonlinear wave mixing with a strong energy exchange which is decisive for a wide range of applications in nonlinear optics [2]. The photorefractive response depends on the state of the polar structure, increases with increasing spontaneous polarization $\mathbf{P}_s$, and shows hysteresis-like behaviour under an external electric field E_0 as a result of the conventional ferroelectric hysteresis $\mathbf{P}_s(E_0)$ [3, 4]. In its turn, the polar structure can be influenced by photoelectric currents and space-charge fields induced in the crystal bulk during the formation of photorefractive gratings [5, 6]. Such a feedback between photorefractive and ferroelectric properties is of great interest for applications like the photoassisted fabrication of certain domain structures or hologram fixation in photorefractive crystals [7].

Highly Ce-doped $Sr_{0.61}Ba_{0.39}Nb_2O_6$ (SBN:Ce) is an illustrative material for studying ferroelectricity-dependent properties of the photorefractive response as well as photoassisted effects in the polar structure of ferroelectrics. Doping with cerium considerably lowers

the phase transition temperature from the low-temperature ferroelectric phase (point group $4mm$) into the high-temperature paraelectric phase (point group $4/mmm$) [8, 9]. The relaxor properties of SBN result in a strong *smearing* of the polar decay over a quite extended temperature interval [10]. As a result, even a moderate increase of the crystal temperature can strongly affect ferroelectric and photorefractive properties. One way to bring about a temperature increase is an illumination with a laser beam.

Recently, it was shown that the effect of photo-induced light scattering (beam fanning) can be successfully applied to study ferroelectric and photorefractive properties of SBN [11, 12]. The scattering is usually attributed to a nonlinear enhancement of the optical coherent noise at the expense of the pump beam due to two-wave mixing on photorefractive noisy gratings [13]. A simple photorefractive model can give a sufficiently explicit description of most properties of photo-induced light scattering in SBN in a very wide temperature interval if the relation between ferroelectric and photorefractive properties is taken into account. It was shown that the scattering can be an effective tool for the evaluation of the phase transition temperature and for the study of the thermal evolution of the polar structure undergoing a phase transition [14, 15].

In this paper we present a study of intensity dependent properties of the scattering in highly doped SBN:Ce without and with externally applied electric fields. Due to the strong light absorption, a remarkable increase of the crystal temperature even up to the phase transition occurs. Therefore noticeable changes of the ferroelectric and photorefractive properties of SBN in the illuminated region result. At first we briefly review different models of the scattering effect and its dependence on the ferroelectric properties of SBN, which are applied in the discussion of the experimental results. The experimental set-up section gives the necessary details of the sample and the measurement itself. In the main section, the peculiarities of the scattering process at high and low light intensities are studied in detail and are explained by the influence of temperature changes on the photorefractive effect. It is shown that the scattering may serve for an evaluation of the crystal temperature in the illuminated area. The effect of the local spontaneous reorientation of the scattering pattern is reported and attributed to a local reversal of ferroelectric domains in the area optically heated up close to the phase transition.

2. Background

Propagation of an extraordinarily polarized laser beam in photorefractive ferroelectrics with nonlocal response is accompanied by the nonlinear optic effect of wide-angle scattering characterized by the appearance of a pronounced asymmetry in the spatial distribution of intensity, as shown in figure 2. There are two basic models explaining the origin of this effect.

The beam fanning model proposed by Feinberg interprets the scattering as asymmetric self-defocusing of the incident beam on a self-induced refractive-index structure. The three-dimensional structure of this refractive-index change is suggested as a cylindrically radial surface with a asymmetric (prism-like) profile in the transverse plane [16]. The beam is self-fanned (or self-deflected) on phase gratings with $\mathbf{K}_{pij} = \mathbf{k}_{pi} - \mathbf{k}_{pj}$ recorded via the photorefractive effect by different beam components $\mathbf{k}_{pi}$ and $\mathbf{k}_{pj}$ composing the Gaussian beam profile. Every single photorefractive grating is a result of a transformation of the corresponding elementary interference pattern into a spatial modulation of the index of refraction by the photo-induced space charge field E_{sc} via the largest linear electro-optic coefficient in SBN r_{33}, $\Delta n = -0.5 n_e^3 r_{33} E_{sc}$. The field E_{sc} is yielded by photoexcited electric carriers migrating from bright to dark regions. Because diffusion of electrons is the dominant charge transport in SBN, photorefractive gratings are shifted by a quarter-period. The unidirectional energy exchange via two-wave mixing processes with the coupling constant $\Gamma = 4\pi \Delta n / \lambda$ causes the angular asymmetry of beam fanning.

The photo-induced light scattering model, first proposed by Voronov *et al* [13], also involves the photorefractive two-wave mixing approach. However, there the scattering effect is explained as the nonlinear enhancement of the optical coherent noise components $\mathbf{k}_{sj}$ at the expense of the laser beam $\mathbf{k}_p$ due to the effective energy coupling on photorefractive gratings $\mathbf{K}_{sj} = \mathbf{k}_p - \mathbf{k}_{sj}$. The detailed theoretical description of this model applied for SBN can be found in [17]. In the following, we will keep this model as it is valid for a much larger interval of scattering angles than the beam fanning model and fits better to our experimental results. We consider the scattering in SBN as the result of the number of two-wave mixing processes between the incident beam and various components of the initial scattering (optical noise) propagating at different angles θ_s measured from the normal and ranged from $-90°$ to $+90°$. The most pronounced refractive index changes are induced via the electro-optic coefficient r_{333} along the polar c axis, just as in the beam fanning model. The $\pi/2$-shift of gratings provides amplification of scattering components in the $-c$ direction and depletion in the $+c$ direction:

$$I_s^{\pm c} = I_{so}^{\pm c} \exp(\mp \Gamma l), \tag{1}$$

where I_{so} and I_s are the initial and steady state scattering intensities, respectively. I_{so} determines the primary scattering of the laser beam on surface and bulk optical inhomogeneities of the crystal. Recent studies of the primary scattering in SBN show that bulk variations of the refractive index imprinted in the domain structure can be associated with such initial scattering sources [12, 18].

The coupling length l in equation (1) is usually identified with the crystal thickness. An expression for the two-wave mixing coefficient Γ is

$$\Gamma(\theta_s) \approx \frac{n_e^4 e\, r_{33} \sin\theta_s \cos^2\theta_s}{\frac{\lambda^2 e^2}{4\pi^2 k_B T} + \frac{4\varepsilon_{33}\varepsilon_0 \sin^2\theta_s}{N_{eff}}}, \tag{2}$$

where k_B is the Boltzmann constant, e is the unit charge, N_{eff} is the trap density, λ is the wavelength, n_e is the extraordinary index of refraction, T is the crystal temperature, and ε_{33} and ε_0 are the dielectric permittivity and dielectric constant.

Beam fanning and photo-induced light scattering are terms applied in the literature to define the same effect. However, for brevity the first term is often used instead of the second one regardless of their primary meaning. In order to avoid further confusion in the text, we will prefer photo-induced light scattering, because as we believe (also it will be shown in section 5) the term explains better the experimental results.

In SBN the relation between r_{33} and $P_3 = P_s$ can be written as [19]

$$r_{33} = 2g_{33}P_s\varepsilon_{33}\varepsilon_0, \tag{3}$$

where g_{33} is the quadratic electro-optic coefficient. Hence, the efficiency of the two-wave mixing and the scattering intensity depend on the modulus of the vector $\mathbf{P}_s$. In addition, the direction of the energy exchange and spatial orientation of the scattering pattern depend on the direction of $\mathbf{P}_s$. By this, the spatial and intensity properties of the scattering may serve as a measure for the state of the polar structure.

To extend the photorefractive model of photo-induced light scattering to elevated temperatures close to the ferroelectric–paraelectric phase transition, the strong relaxor properties of SBN have to be taken into account. There are different models [20–22], which describe different relaxor scenarios in SBN. They all assume that at high temperatures the polar structure can be considered as an assembly of polar clusters—local areas in the crystal with nonzero electric polarization. Gradual thermal decay of clusters results in a strong smearing of the phase transition. One peculiarity of SBN is the very rich variety of ferroelectric domains of different sizes observed in the crystal bulk [23]. Such strong fragmentation of the polar

structure is caused by internal fields of local charge centres existing in the crystal bulk, possibly due to the incommensurate structure of SBN [24]. The random arrangement of internal fields in as-grown SBN results in a spatial distribution of domains randomly oriented either along or opposite to the z-axis. Electric poling of SBN by the field cooling technique (FC poling), i.e. a high external field is applied in the paraelectric phase and remains on the sample until it is cooled down to the ferroelectric phase, imposes the same spatial order in ferroelectric domains and in the distribution of local internal fields in the bulk [25, 26]. This is because, at high temperatures, the mobility of local charge centres is rather high, and they arrange according to the external field. The FC-poled SBN resembles a stable system of highly ordered and mutually matched spatial structures of domains and internal fields imprinted into the crystal bulk. Further repoling of the crystal by external fields at room temperature is sufficient to reverse the spontaneous polarization $\mathbf{P}_s$ by an inversion of ferroelectric domains, but cannot change the arrangement of internal fields. This spatial mismatch between domain and internal field structures results in the reduced stability of the polar structure with respect to further changes of experimental conditions. One consequence of this is the asymmetry of the coercive field [27]. Another is the fatigue of the ferroelectric $P_s(E_0)$ hysteresis [28], a result of the so-called pinning effect [27], when during the electric repoling some domain walls are pinned by internal fields, preventing further domain reversals under external fields. At the same time, some softening of the fatigue effect may occur from the induced photoconductivity during the optical illumination of the crystal, because free electrons partially compensate an action of the internal fields [12, 29, 30].

3. Experimental set-up

Measurements were performed with a $Sr_{0.61}Ba_{0.39}Nb_2O_6$ crystal doped with 0.66 mol% cerium grown by the Czochralski technique. Its input face with dimensions $a \times c = 5.6 \times 2.8$ mm^2 was polished to optical quality. The thickness was $l = 0.7$ mm. The ferroelectric–paraelectric phase transition is detected at $T_M = 52\,°C$ [14]. An FC poling was performed to obtain a sample with nonzero polarization in the ferroelectric phase: the crystal was heated up to 140 °C and then cooled back to room temperature under an applied electric field of $E_0 = 3.5$ kV cm^{-1} along the polar c axis. Considerable changes of the coefficients r_{33} and ε_{33} are measured already not far from room temperature [11, 31]. Since highly doped SBN:Ce is characterized by large optical absorption, it is obvious to expect local changes of the temperature and material parameters under intense illumination in the sample.

The principle of our optical investigations is shown schematically in figure 1. The crystal was placed on a thermoelectric element allowing temperature control in the range from 10 to 150 °C with an absolute accuracy of 0.01 °C. The crystal was originally oriented so that the spontaneous polarization $\mathbf{P}_s$ coincides with the coordinate z. Both c-surfaces are connected to a dc power supply in order to apply the electric fields to the sample within the set-up. An electric field of $E_0 = 3.5$ kV cm^{-1} was chosen, much larger than the coercive field $E_{cr} = 1.5$ kV cm^{-1}. Fields with the same polarity as the one used during FC poling are considered as positive.

The SBN crystal was illuminated by an unexpanded pump beam of a frequency-doubled Nd:YAG laser (type Compass 315-M, Coherent) operating at $\lambda = 532$ nm with a beam diameter of $d_{FWHM} = 1.5$ mm. The laser beam of extraordinary light polarization impinged normally to the input face of the sample. The measurements were performed with two different intensities: (a) the low-intensity case with $I_p = 3.5$ kW m^{-2} and (b) the high-intensity case with $I_p = 35$ kW m^{-2}. With an absorption coefficient of $\alpha(\lambda = 532\text{ nm}) = 28.6$ cm^{-1} the low-power beam does not significantly influence the crystal temperature, while the high-power beam strongly heats the illuminated volume.
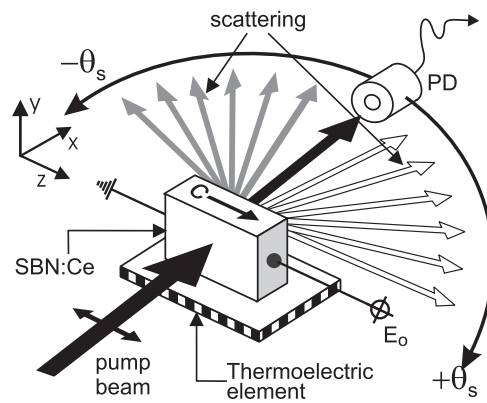
Figure 1. Experimental set-up for measuring the angular distribution of scattered light in SBN:Ce. PD is a photodiode mounted on a rotating stage. The crystal is placed on a stack of Peltier elements to control the temperature.
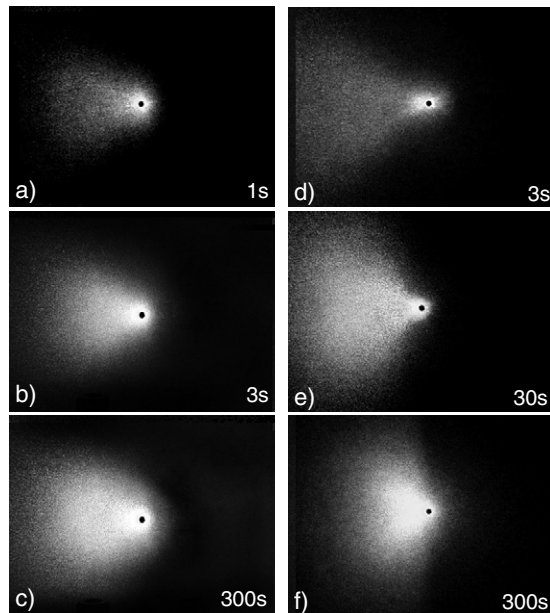
Figure 2. Scattering pattern on a screen behind the crystal at different moments of its evolution: (a)–(c) are for $I_p = 3.5$ kW m^{-2}, (d)–(f) are for $I_p = 35$ kW m^{-2}.

Photographs of the scattering pattern were taken at a viewing screen. To measure the angular intensity distribution in the scattering pattern along the z axis, a photodetector PD was mounted on a motorized rotation stage at a distance of $L = 10$ cm from the sample and rotated in the direction from $-z$ to $+z$ in the angular range of $-90° \leqslant \theta_s \leqslant +90°$, measured in air. Negative ($-\theta_s$) and positive ($+\theta_s$) scattering angles correspond to $-c$ and $+c$ directions, respectively. The scattering angle corresponding to the direction of propagation of the pump beam was defined as $\theta_s = 0°$. The photodetector aperture limits the resolution of the apex angle of the measured light to $0.5°$. To measure the temporal evolution of scattering, two photodetectors with angular apertures of $4°$ were used symmetrically mounted with respect to
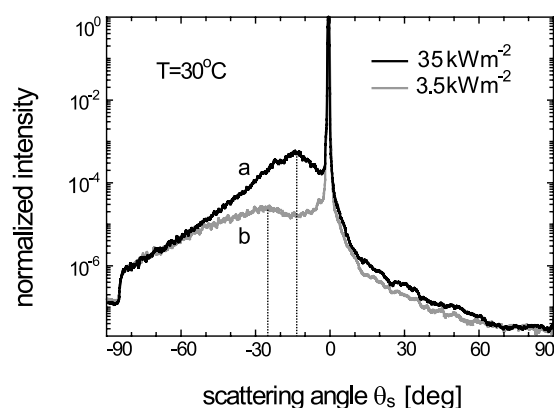
Figure 3. Angular distribution of the scattered light at high (a) and low (b) pump intensity.

the pump beam. The entire set-up was placed within a black box with a small window for the pump beam in order to minimize the incoherent optical noise.

4. Intensity dependent study of scattering

Experimental results and discussion of intensity dependent properties of scattering in SBN are divided into two parts. The subject of the first part is the influence of the pump beam intensity on scattering processes in the crystal with highly stable state, i.e. the mutual arrangement of the polar structure and internal fields is not perturbed. For this, the scattering is studied when *no external electric fields* are applied to the crystal. In the second part, the SBN crystal under the additional action of *high external fields* is considered. This allows the study of the intensity dependent scattering in the case of the crystal in the perturbed state, when spatial alignments of ferroelectric domains and internal electric fields are mutually mismatched. In both cases, temporal and steady state characteristics of the scattering are measured. In the second part, the effect of spontaneous reorientation of the scattering pattern is reported and discussed.

4.1. No external fields

Figure 2 shows the development of scattering in SBN as a function of time induced with low (2(a)–(c)) and high (2(d)–(f)) pump beam intensities. Since the direction of the polar axis coincides with the $+z$-axis of the coordinate system, a pronounced scattering distribution is observed on the left-hand side (negative angles, $-z$-scattering), whereas it is hardly visible on the right-hand side (positive angles, $+z$-scattering) in accordance with equation (1). The scattering intensity in $-z$-direction continuously increases for the low-intensity case and saturates without qualitative changes in its spatial intensity distribution. In contrast, for the high-intensity case the scattering distribution first extends to large scattering angles (2(d) and (e)) but contracts to smaller apex angles θ_s after longer times (2(f)).

For both cases the intensity distribution of the scattering pattern was scanned in the direction parallel to the *c*-axis in order to examine the steady state ($t = 600$ s) differences in more detail. Figure 3 shows the intensity of the scattered light I_s as a function of the apex angle θ_s for an illumination with $I_p = 35$ kW m^{-2} (curve a) and $I_p = 3.5$ kW m^{-2} (curve b). The intensities are normalized to the intensity of the respective transmitted laser beam at $I_s(\theta = 0°)$. Obviously the intensity of the scattered light is higher for curve (a) compared
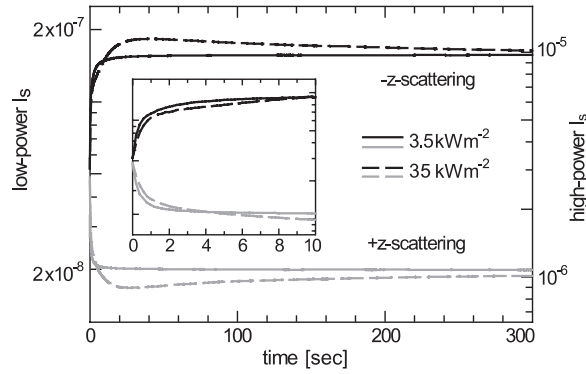
Figure 4. Dynamics of $\pm z$-scattering in SBN:Ce at $\theta_s = \pm 30°$ ($I_p = 3.5$ kW m^{-2}, solid curves) and $\theta_s = \pm 15°$ ($I_p = 35$ kW m^{-2}, dashed curves). The inset shows an enlarged view of the first ten seconds.

to curve (b) and the maximum of the scattering intensity distribution is shifted to smaller angles. Scattering induced with intensities of the pump beam deviating from $I_p = 3.5$ kW m^{-2} showed identical intensity distributions as in (b), while deviations from the pump intensity $I_p = 35$ kW m^{-2} result in further changes in the scattering pattern shape. Therefore, we conclude that the photorefractive properties of the crystal are unaffected in the low-intensity case but are strongly affected in the high-intensity case.

In addition the intensity of the scattered light was measured as a function of time at a fixed scattering angle in order to monitor the temporal evolution of the scattering in $-z$- and $+z$-directions (figure 4). Two stationary photodiodes were placed symmetrically at $\theta_s = \pm 30°$ for the low-intensity case (continuous line) and $\theta_s = \pm 15°$ for the high-intensity case (dashed line), respectively. Thus the intensity was especially detected in the maximum of the scattering distribution in the $-z$-direction (see figure 2). The inset of figure 4 shows the beginning of the build-up within the first ten seconds. It can be seen that the intensity of the scattered light is identical at $t = 0$ for $\pm\theta_s$. Saturation of the scattered light is already reached after ten seconds in the low intensity case and remains constant for further exposure. In contrast, using a ten times stronger pump beam intensity of $I_p = 35$ kW m^{-2} the intensity of the scattered light exhibits a maximum after about 30 s and decreases slightly following further time until a steady state is reached at about 600 s.

4.2. High external fields

Two different cases of external application of electric fields to the sample have been investigated.

- *Separate application of external field and illumination* (A-procedure). An external field E_0 is applied to the non-illuminated crystal for 10 s and then switched off. After a relaxation time of 1–2 min, the crystal is illuminated.
- *Simultaneous application of external field and illumination* (B-procedure). An external field E_0 is applied to the non-illuminated crystal for 10 s, then the pump beam is switched on. The field remains applied during the illumination of the crystal.

A negative electric field $E_0 = -4$ kV cm^{-1} applied according to the A- or B-procedure should reverse the spontaneous polarization P_s and therefore the scattering direction. Any decrease or increase of the reversed spontaneous polarization caused by incomplete reversal of
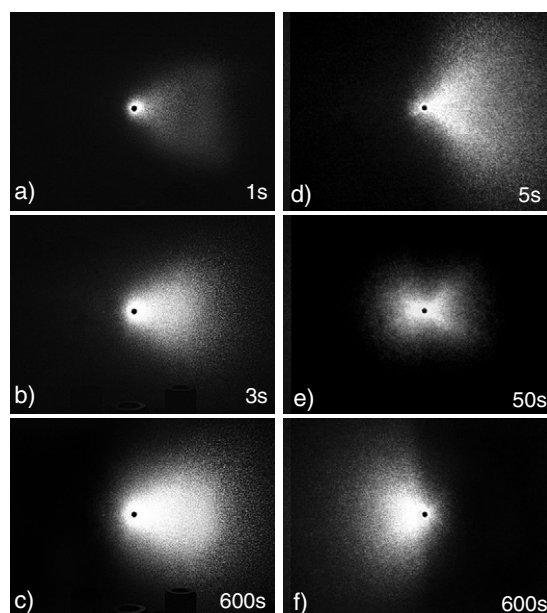
Figure 5. Scattering pattern in SBN at different times after application of the external field $E_0 = -4$ kV cm^{-1} by the A-procedure: (a)–(c) are for $I_p = 3.5$ kW m^{-2}, (d)–(f) are for $I_p = 35$ kW m^{-2}.

ferroelectric domains will be indicated by the corresponding intensity changes of the scattering pattern [12, 15].

Figure 5 shows photographs of scattering in SBN:Ce illuminated after the application of the external field (A-procedure) for the low-intensity ((a)–(c)) and high-intensity ((d)–(f)) cases. At low intensities, the illumination does not affect the new orientation of domains. The scattering pattern smoothly develops in the $+z$-direction. However, a completely different behaviour occurs at high intensities. First, the scattering pattern develops in the $+z$-direction (5(d)), then collapses into symmetric small-angle scattering around the transmitted beam (5(e)), and afterwards develops in the $-z$-direction (5(f)) originally set by the FC poling as the $-c$-direction. This new effect of the local spontaneous reorientation of the scattering pattern will be discussed in more detail in the next section. Results almost like those in figure 5 are observed if the sample is optically illuminated during the application of the external field (B-procedure). As well as in the originally poled sample, the scattering reaches the steady state faster at low intensities compared to that at high intensities. For the low-intensity case, the scattering dynamics corresponding to the A- and B-procedures are shown in figures 6(a) and (b), respectively. The intensity was measured at angles $\theta_s = \pm 30°$. As one can see, photo-induced light scattering keeps the new direction defined by the applied field, and scattering reversal by the B-procedure is more efficient than that by the A-procedure. The maximum is reached immediately after the first application of the field (the solid and dashed curves in figure 6(b) almost coincide) with the B-procedure and only after the third application with the A-procedure. This difference is similar to that reported for scattering reversal at $\lambda = 633$ nm [15]. Respectively, the scattering dynamics for A- and B-procedures for the high-intensity case are shown in figures 7(a) and (b) measured at $\theta_s = \pm 15°$. In contrast to figures 6(a) and (b), here again the spontaneous reorientation of the scattering pattern back to
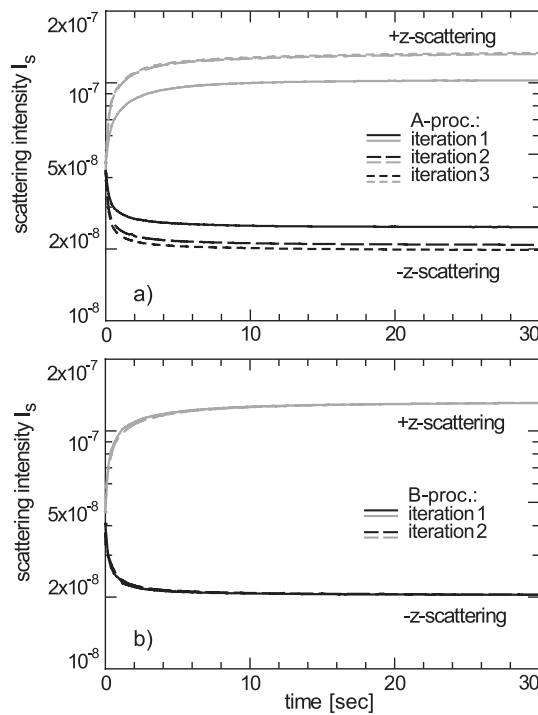
Figure 6. Dynamics of scattering at $\theta_s = \pm 30°$ ($\pm z$-scattering) in SBN:Ce after the external field $E_0 = -4 \text{ kV cm}^{-1}$ applied by the A-procedure (curve a) and B-procedure (curve b); for details see the text. The intensity of the pump beam is $I_p = 3.5 \text{ kW m}^{-2}$ (low-intensity illumination).

the $-z$-direction occurs opposite to the direction of the external field. Another peculiarity of the scattering at high intensities is the locking effect also shown in figure 7. If the field is applied repeatedly, the scattering pattern does not switch at all to the $+z$-direction but remains locked in the $-z$-direction despite the external fields. This locking is more effective for procedure B than for procedure A. One-time application of a positive external field unlocks the scattering. Afterwards, a negative field can again switch the scattering direction. The new dynamics are again equivalent to the curves in figure 7, and the locking starts anew.

5. Discussion

5.1. Scattering without external fields

The scattering dynamics shown in figure 4 are an important method for verifying the validity of the beam fanning and photo-induced light scattering models [13, 16]. The experimental observation of simultaneous suppression and amplification of the coherent noise respectively in positive and negative directions of the polar c axis, for the first time reported in our experiment, shows a very good agreement with predictions of equation (1). The evident temporal synchronism detected at rather large scattering angles far from the transmitted laser beam gives evidence for the validity of the photo-induced light scattering model. From two mutually symmetric components of the coherent optical noise, one will be amplified and the other depleted depending on the sign of the scattering angle but regardless of its module. It is valid for all scattering angles $-90° \leqslant \theta_s \leqslant +90°$. At the same time, the beam fanning
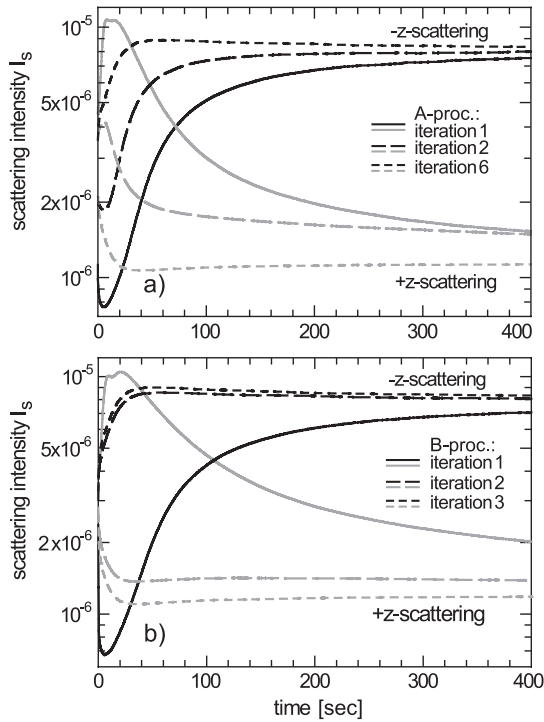
Figure 7. Dynamics of scattering at $\theta_s = \pm 15°$ ($\pm z$-scattering) in SBN:Ce after application of $E_0 = -4$ kV cm^{-1} by the A-procedure (curve a) and the B-procedure (curve b). The intensity of the pump beam is $I_p = 35$ kW m^{-2} (high-intensity illumination).

model predicts different angular intervals where the signal will be enhanced and reduced. The intensity increases in the direction of the beam deflection defined by the slope of the refractive index profile, while angles of depletion are limited by the Gaussian divergency of the laser beam and therefore are much smaller than the scattering angles used in the experiment. Taking into account that the phenomena investigated in this paper are related to large scattering angles, the usage of the photo-induced light scattering model seems to be more appropriate.

A comparison of main features of the scattering shown in figures 2–4 suggests that the high-intensity illumination strongly influences the photorefractive and ferroelectric response of SBN, but the polar structure induced in the crystal by FC-poling remains stable. To explain the difference in the properties of scattering induced by the high-power and low-power laser beam, we should take into account a possible effect of crystal heating via the optical absorption in the former case. We assume that transient longitudinal and radial temperature gradients arise along and across the beam path immediately after the illumination begins. However, then the gradients are gradually equalized. The high thermal conductivity (1.71 W m^{-1} K^{-1} ∥ a [32]) provides an effective redistribution of the temperature changes through the sample. At the same time, the smaller thermal conductivity of air slows a further transmission of the light-induced heat from the crystal surface to air, because a heat flow is substituted here by a natural convection. This will finally result in significant homogenization of the temperature profile in the whole sample, and particularly in the rather thin illuminated volume. The temperature increase can be roughly estimated as follows. The sample absorbs about 87% of the laser beam, corresponding to an energy input of $Q_{in} = 46$ mW in the high-intensity case. Losses

Q_{out} are due to (i) heat conduction from the sample to the Teflon holder, (ii) heat convection and (iii) radiation to air. At the actual experimental conditions, the convective heat transfer from the sample to air is the most important factor. It is proportional to the surface area S and the temperature difference ΔT between the surface and air, and is described by Newton's law:

$$Q_{out} = hS\Delta T, \tag{4}$$

where h is the free-convection heat transfer coefficient specific for the particular experimental conditions[5]. An equilibrium between the sample and air occurs for $Q_{in} = Q_{out}$, resulting in $\Delta T \approx 70\,°C$ as an upper limit of the homogeneous temperature increase in the sample. For the sample initially being at room temperature, this corresponds to a heating above the phase transition temperature. On the other hand, some lowering of ΔT is expected due to two other channels of energy dissipation mentioned above.

According to the SBN features mentioned in section 2, a strong light-induced heating should influence ferroelectric as well as photorefractive properties of the relaxor SBN. Obviously, the changes are most perceptible if the laser beam is indeed able to heat the crystal close to the phase transition. The dependence of scattering properties on the light intensity can be explained by the temperature dependence of the two-wave mixing coefficient Γ. In accordance with equation (2), Γ directly depends on T, especially due to the temperature dependence of r_{33} and ε_{33}. An influence of $n_e(T)$ and $N_{eff}(T)$ can be excluded in the first approximation, since temperature induced changes of the refractive index are negligible [34], and noticeable changes of N_{eff} occur only above the phase transition [11]. Note, that the temperature T and all temperature dependent material parameters in equation (1) can be considered as values averaged over the illuminated volume. The parameters r_{33} and ε_{33} enter equation (2) in the numerator and denominator, respectively. Only these two parameters define the angular distribution of Γ along the z-axis, and particularly the angular position of its maximum. With respect to the known temperature dependence of r_{33} and ε_{33} [11, 31] we expect the maximum of Γ at smaller scattering angles with increasing temperature. Thus the different scattering profiles for the low and high intensity case (figure 3) can be explained, since different strengths of the temperature change are induced by the pump beam. In the low intensity case this temperature change can be neglected.

Likewise, we can explain the transient behaviour of the scattering at high intensities (figure 4). As the sample heats up during the illumination, the maximum of the scattering pattern moves from 25° to 12°, crossing the photodiode at 15°.

It has to be emphasized that the intensity and temperature dependencies of the scattering profiles measured in the experiment exhibit qualitatively similar behaviour with a very good repeatability for different SBN samples of the same doping concentration and stoichiometry. This is warranted by the high reproducibility of the material parameters r_{33} and ε_{33} defining the angular dependence of the coupling coefficient Γ. According to this experimental result, the temperature increase induced by $I_p = 35\ \mathrm{kW\,m^{-2}}$ can be evaluated from the temperature dependence of the scattering distribution measured from the weak pump beam in the homogeneously heated crystal using thermoelectric elements. Therefore, the low-intensity measurements ($I_p = 3.5\ \mathrm{kW\,m^{-2}}$) of the angular distribution of scattering at different temperatures have been performed in the same SBN sample. Some scattering profiles are shown in figure 8. An increase of the overall scattered intensity is observable up to the phase transition temperature of $T = 52\,°C$ accompanied by a shift of the maximum of the intensity distribution closer to the pump beam. The resulting temperature dependence of $\theta_s(I_s^{max})$, measured for the

---

[5] For the vertical crystal plate of height L, the free-convection heat transfer coefficient is satisfactorily described by a simple relation $h = 1.42\left(\frac{\Delta T}{L}\right)^{1/4}$ [33]. The relation is empirical and L has to be inserted in metres, while h preserves its typical unit $\mathrm{W\,m^{-2}\,°C^{-1}}$.
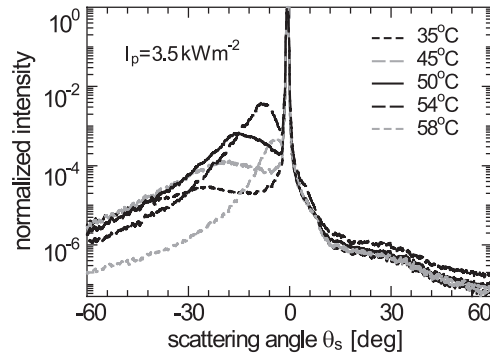
Figure 8. Angular distributions of scattered light at various sample temperatures (I_p = 3.5 kW m^{-2}).
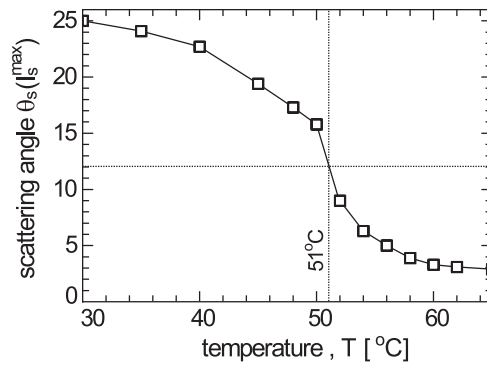
Figure 9. Angular position of the scattering maximum versus the crystal temperature for I_p = 3.5 kW m^{-2}.

low-intensity case, is shown in figure 9. The maximum of the high-intensity profile measured at I_p = 35 kW m^{-2} is at the angle $\theta_s(I_s^{max})$ = 12° (see curve (a) in figure 3). According to figure 9 this angle corresponds to an effective crystal temperature of T = 51 °C.

5.2. Scattering at high external fields

The scattering pattern reversal shown in figures 5(a)–(c) and 6 indicates that the reversed arrangement of the polar structure in SBN remains stable at low pump intensities. The direction of the energy transfer between pump and scattering waves has changed from the $-z$- to the $+z$-direction, since the polar axis is now aligned along $-z$. Thus, the $+z$ scattering is now amplified, while the $-z$ scattering is depleted. It indicates that the influence of low-intensity coherent illumination on the polar structure does not go beyond the suppression of the fatigue effect via the generation of free photoelectrons into the conduction band. The higher efficiency of the scattering reversal by the B-procedure compared to that by the A-procedure can be explained due to the drift of photocarriers in the external field contributing to compensation of internal fields additionally to the diffusion processes [15]. Note that the compensation is only successful if the external field increases faster than the screening field at the border of the illuminated area.

The new effect of spontaneous reorientation of the scattering pattern against the action of the external field is observed only at elevated intensities. This phenomenon is different from the conventional scattering reversal, which always follows the direction of an externally applied electric field [15]. The spontaneous reorientation of the scattering indicates that the coefficient Γ switches its sign opposite to that defined by the applied field. According to equation (2), the sign of Γ is defined by the sign of the electric photocarriers and the linear electro-optic coefficient r_{33} (see equation (2)). Since electrons remain the dominating electric photocarriers in SBN, it is obvious to conclude that r_{33} changes sign, which can be a result of the spatial inversion of the spontaneous polarization $\mathbf{P}_s$ against the action of the external field. We attribute this effect to the action of the internal electric fields on ferroelectric domains in which new spatial orientation is induced by the negative external field and occurs mismatched with respect to the FC-imprinted distribution of internal fields. At low intensities of the pump beam, the reversed orientation of the polar structure remains rather stable and is not affected by the internal fields. When the high-intensity pump beam significantly increases the crystal temperature, the impact of the internal fields increases. However, since the dielectric relaxation time τ_{di} is smaller than the specific time of the heating process, the scattering develops in the $+z$ direction defined by the negative external field (figure 5(d)). With increasing temperature in the illuminated region, the coercive field is reduced and the domains become more and more sensitive to the action of the internal fields. If the temperature reaches a value where internal fields equal the coercive field, half of the domains are switched back to the direction imprinted by the FC poling. The scattering collapses, and only some temporal small-angle scattering caused by large-sized domains near to the pump beam is observed (figure 5(e)). This indicates a heterogeneous state of the polar structure. A further increase of the temperature leads to the switching of the rest of the domains to the predefined orientation within the illuminated region. Ferroelectric domains and internal fields hence constitute a mutually matching spatial distribution, and the scattering appears again in the $-z$-direction (figure 5(f)). Therefore, our study shows that the new order in the polar structure made by external fields at room temperatures becomes locally unstable with respect to actions of internal fields in the crystal area illuminated by high-intensity beams. The action of internal fields is aimed to restore the spatial matching between internal fields and ferroelectric domains initially imposed by FC poling.

An interesting point is that the process of spontaneous reorientation becomes more effective in the presence of the external field (B procedure). The drift of photoelectrons in the external field immediately results in the formation of a strong field at the beam border opposite to the direction of the external field. This field compensates the external field E_0 and greatly assists the internal fields to restore the ferroelectric domains within the illuminated area to the initial orientation. The experiment confirms the promotion of the spontaneous reorientation of the scattering back to the initial state in the presence of high external fields. At the same time, the existence of the compensating field is a secondary factor, since the reorientation also occurs when the external field is switched off (A procedure). Actually, the effect of spontaneous domain back-switching over the entire crystal was earlier reported in pulse poled ferroelectrics [35, 36]. To check if the domains in the non-illuminated areas of our sample are also reversed back, we probed these areas with a low-power beam. We found the scattering in the $+z$-direction, proving that the polar structure remains stable there. The effect of locally reoriented scattering cannot be observed if SBN is poled at room temperature after zero-field cooling, since this technique does not imprint a spatial order of the local fields in the crystal bulk. Therefore, in the case of the spontaneous reorientation of the scattering we deal with a local spatial reversal of ferroelectric domains brought about by the spatially ordered internal fields. It should be noted that the highly pronounced spatial features of the

spontaneous reorientation of the scattering distinguish this effect unambiguously from the effects of 'switching' and 'back-switching' of the inelastic scattering in PLZT ceramics under the action of rectangular field pulses [37].

The spatial locking of the scattering illustrated by the scattering dynamics in figure 7 can be explained by effects of the damping field and the pinning on domain walls. The damping field is formed at the pump beam border. During the first application of the external field, all domains switch their orientation. During the high-intensity illumination, the domains in the illuminated area switch back, but the domains in the dark areas do not. Thus, the border of the pump beam becomes the frontier between differently oriented domains. The local fields at the domain walls are compensated by photoexcited electrons, forming a screening field around the beam. This field remains in the crystal even after the illumination is finished, partially hindering a further spatial domain reversal with the external fields. At the same time, possibly because of the increased mobility of the local charge centres at high temperatures [26], the internal fields cannot be compensated completely by photoelectrons. Therefore, domain walls still can be pinned by the internal fields. This pinning reduces the number of switchable domains, until the locking of the domains in the direction of the primary FC poling is completed.

It could be expected that the spontaneous reorientation of the scattering should be observed in homogeneously heated SBN crystals, also. However, as reported in [15] this effect does not occur when the sample is heated by a resistor up to $T > T_m$ and is illuminated by a low-intensity beam of wavelength $\lambda = 633$ nm. Thus the local heating by the pump beam plays a decisive role for the appearance of the effect. We assume that the homogeneous heating does not result in the creation of charged domain walls, and therefore damping fields do not arise in the crystal. Furthermore, the space-charge fields, which are induced by the photorefractive effect, are significantly stronger for the shorter light wavelength.

Here we should note that the processes responsible for the local spontaneously reoriented scattering are different from the processes resulting in the photo-assisted transformation of photorefractive gratings into domain gratings. The growth of such domain gratings is caused by the repoling of the crystal with a spatially modulated field, which is referred either to the photorefractive space-charge field induced by two coherent beams of nearly equal intensities [6], or to the sum of a photorefractive field and a moderate external field slightly lower or higher than the coercive field [38–44]. In the case of scattering, the small modulation depth of the interference patterns made by the weak seed and strong pump waves does not result in large space-charge fields sufficient to inverse the polar structure. Moreover, the effect of these photorefractive fields on the polar structure is negligible compared to the action of the high external field.

6. Conclusion

In conclusion, intensity dependent properties of photo-induced light scattering were studied in ferroelectric SBN:Ce. A comparative study of dynamic and steady state properties of the scattering from low- and high-intensity pump beams has been performed. It is shown that the scattering at high intensities exhibits anomalous changes, like the increased time of the development and a strong restraint of the angular distribution. These features are traced back to the heating of the crystal by the pump beam from room temperature close to or even above the phase transition temperature, resulting in changes of material properties and influencing the photorefractive coupling coefficient Γ. A comparison of the scattering in the crystal with and without high externally applied electric fields E_0 reveals the instability of the scattering pattern at elevated pump intensities manifested by a spontaneous reversal of the scattering pattern against the action of the external field. This new effect appears even if the crystal

is illuminated after the application of the external field. It is explained as the result of local back-switching of the spontaneous polarization due a thermal lowering of the coercive field in the illuminated area via the optical absorption, and increased action of internal fields causing a reversal of ferroelectric domains back to the direction imprinted by the initial FC poling. The detailed analysis of the related processes requires a simultaneous account of the mutual influence of coherent illumination and material properties of the crystal as well as of relaxor properties of the polar structure, which are increasing with the temperature.

Acknowledgment

References

[1] Kukhtarev N, Markov V, Odoulov S, Soskin M and Vinetskii V 1979 *Ferroelectrics* **22** 961
[2] Yeh P 1993 *Introduction to Photorefractive Nonlinear Optics* (New York: Wiley)
[3] Ma J, Liu L, Wu S, Xu L and Shu B 1988 *Appl. Phys. Lett.* **53** 826
[4] Woike Th, Volk T, Dörfler U, Pankrath R, Ivleva L and Wöhlecke M 1998 *Ferroelectr. Lett.* **23** 127
[5] Prokhorov A and Kuz'minov Yu 1990 *Ferroelectric Crystals for Laser Radiation Control* (Bristol: Hilger)
[6] Kewitsch A, Segev M, Yariv A, Salamo G, Towe T, Sharp E and Neurgaonkar R 1994 *Phys. Rev. Lett.* **73** 1174
[7] Kewitsch A S, Yariv A and Segev M 1995 *Permanently Fixed Volume Phase Gratings in Ferroelectrics in Photorefractive Effects and Materials* ed D Nolte (Boston, MA: Kluwer Academic)
[8] Volk T, Woike Th, Dörfler U, Pankrath R, Ivleva L and Wöhlecke M 1997 *Ferroelectrics* **203** 457
[9] Granzow T, Woike Th, Rammensee W, Wöhlecke M, Imlau M and Pankrath R 2003 *Phys. Status Solidi* A **197** R2
[10] Kuroda S and Kubota K 1980 *J. Phys. Chem. Solids* **42** 573
[11] Goulkov M, Granzow T, Dörfler U, Woike Th, Imlau M and Pankrath R 2003 *Opt. Commun.* **218** 173
[12] Goulkov M, Granzow T, Dörfler U, Woike Th, Imlau M and Pankrath R 2003 *Appl. Phys.* B **76** 407
[13] Voronov V, Dorosh I, Kuz'minov Yu and Tkachenko N 1980 *Sov. J. Quantum Electron.* **10** 1346
[14] Goulkov M, Imlau M, Pankrath R, Granzow T, Dörfler U and Woike Th 2003 *J. Opt. Soc. Am.* B **20** 307
[15] Goulkov M, Imlau M, Granzow T and Woike Th 2003 *J. Appl. Phys.* **94** 4763
[16] Feinberg J 1982 *J. Opt. Soc. Am.* **72** 46
[17] Obukhovski V and Stoyanov A 1985 *Sov. J. Quantum Electron.* **12** 563
[18] Goulkov M, Shinkarenko O, Granzow T, Woike Th and Imlau M 2004 *Europhys. Lett.* **66** 48
[19] Fox A 1973 *J. Appl. Phys.* **44** 254
[20] Smolenskii G, Isupov V, Agranovskaya A and Popov S 1961 *Sov. Phys.—Solid State* **2** 2584
[21] Burns G and Dacol F 1983 *Phys. Rev.* B **28** 2527
[22] Dec J, Kleemann W, Bobnar V, Kutnjak Z, Levstik A, Pirc R and Pankrath R 2001 *Europhys. Lett.* **55** 781
[23] Fogarty G, Steiner B, Cronin-Golomb M, Laor U, Garrett M, Martin J and Uhrin R 1996 *J. Opt. Soc. Am.* B **13** 2636
[24] Woike Th, Petricek V, Dusek M, Hansen N, Fertey P, Lecomte C, Arakcheeva A, Chapuis G, Imlau M and Pankrath R 2003 *Acta Crystallogr.* B **59** 28
[25] Granzow T, Dörfler U, Woike Th, Wöhlecke M, Pankrath R, Imlau M and Kleemann W 2002 *Appl. Phys. Lett.* **80** 470
[26] Granzow T, Woike Th, Wöhlecke M, Imlau M and Kleemann W 2002 *Phys. Rev. Lett.* **89** 127601
[27] Granzow T, Dörfler U, Woike Th, Wöhlecke M, Pankrath R, Imlau M and Kleemann W 2001 *Phys. Rev.* B **63** 174101
[28] Maciolek R and Liu S 1973 *J. Electron. Mater.* **2** 191
[29] Granzow T, Dörfler U, Woike Th, Wöhlecke M, Pankrath R, Imlau M and Kleemann W 2002 *Europhys. Lett.* **57** 597
[30] Dörfler U, Granzow T, Woike Th, Wöhlecke M, Pankrath R and Imlau M 2004 *Appl. Phys.* B **78** 211
[31] Dec J, Kleemann W, Woike Th and Pankrath R 2000 *Eur. Phys. J.* B **14** 627
[32] Choy C, Leung W, Xi T, Fei Y and Shao C 1992 *J. Appl. Phys.* **71** 170
[33] Holman J P 1986 *Heat Transfer* (New York: Mc Graw-Hill)
[34] Cross L 1987 *Ferroelectrics* **76** 241

[35] Batchko R, Shur V, Fejer M and Byer R 1999 *Appl. Phys. Lett.* **75** 1673
[36] Yu H, Gopalan V, Sindel J and Randal C 2001 *J. Appl. Phys.* **89** 561
[37] Shur V 1998 *Phase Transit.* **65** 49
[38] Micheron F and Bismuth B 1972 *Appl. Phys. Lett.* **20** 79
[39] Qiao Y, Orlov S, Psaltis D and Neurgaonkar R 1993 *Opt. Lett.* **18** 1004
[40] Horowitz M, Bekker A and Fisher B 1993 *Appl. Phys. Lett.* **62** 2619
[41] Cudney R, Fousek J, Zgonik M, Günter P, Garrett M and Rytz D 1993 *Appl. Phys. Lett.* **63** 3399
[42] Kahmann F, Pankrath R and Rupp R 1994 *Opt. Commun.* **107** 6
[43] Smith P and Eason R 1996 *Appl. Phys. Lett.* **69** 1509
[44] Shen X, Zhao J, Wang R, Cheng Z, Zhang Sh and Chen H 2000 *Appl. Phys. Lett.* **77** 1206